East European Journal of Physics. **3.** 93-102 (2025)
DOI:10.26565/2312-4334-2025-3-09 ISSN 2312-4334

SPATIAL DYNAMICS OF A RADIALLY POLARIZED TERAHERTZ LASER BEAM WITH A PHASE SINGULARITY

Andrey V. Degtyarev, Mykola M. Dubinin, Vyacheslav A. Maslov*, Konstantin I. Muntean, Oleh O. Svystunov
V.N. Karazin Kharkiv National University,4 Svoboda Sq., Kharkiv 61022, Ukraine
**Corresponding Author e-mail: v.a.maslov@karazin.ua*
Received April 1, 2025; revised July 21, 2025; accepted August 4, 2025

Analytical expressions are obtained that describe the nonparaxial diffraction in free space of the TM_{01} mode with radial polarization of the field of the dielectric waveguide resonator of a terahertz laser during its interaction with a spiral phase plate with different topological charge (n). The physical features of the obtained vortex beams during their propagation and tight focusing are studied by numerical simulation. The integral diffraction Rayleigh-Sommerfeld transforms are used to simulate the propagation and focusing of the obtained beams. In free space the use of the spiral phase plate at the waveguide output with a topological charge of $n = 1$ leads to a change in the transverse beam profile from annular to a beam that has a field maximum on the axis, and then for $n = 2$ again to annular. During focusing the transverse distribution of the total field intensity in the absence of a spiral phase plate has a ring structure. In this case there is a slight intensity on the axis due to the contribution of the longitudinal component of the field. The transverse profile of the beam changes in the same way as during its propagation when using a phase plate. In this case the phase front changes from spherical to spiral with the presence of two ($n = 1$) and four ($n = 2$) branching vortices.
Keywords: *Terahertz laser; Dielectric waveguide resonator; Spiral phase plate; Vortex beams; Radial polarization; Radiation propagation; Tight focusing*
PACS: 42.55.Lt; 42.60.Da; 42.25.Bs; 47.32.C–

1. INTRODUCTION

Terahertz waves refer to electromagnetic radiation with frequencies in the range of 0.1 THz to 10 THz. These waves have unique characteristics such as high penetrating power, low ionizing power and small scattering. Due to these advantages terahertz waves have broad application prospects in imaging, communication and material characterization [1, 2].

Among the various structural beams vector beams with nonuniform polarization states have shown significant application value in many fields due to their unique light field distribution characteristics. Compared with spatially uniform polarized beams the polarization distribution of vector beams is spatially variable. Due to these properties, vector beams have a number of unique advantages such as precise focusing [3 – 6] and high image resolution [7, 8]. In the optical range, using the Richards-Wolf integral transforms [9 – 11], the features of focusing beams with nonuniform polarization were studied. It is shown that with tight focusing of radially polarized light a circular focal spot is observed. In this case the redistribution of energy between the components of the electric field strength occurs in such a way that the longitudinal component can make a significant contribution to the formation of the focal spot [12, 13].

Another type of structured optical fields with great potential for practical applications are vortex beams. Today optical vortices are used to manipulate microparticles, to enhance image contrast in microscopy, for metrology tasks, and, in particular, to increase the data transmission density in optical communication systems [14 – 17]. The expansion of vortex beam generation techniques into the terahertz (THz) spectral range has been expected to expand the scope of THz technologies. For example, THz vortex beams are attractive for wireless communications because they can support an infinite number of orbital angular momentum eigenstates characterized by their topological charges [18].

The study of the propagation of vortex laser beams in free space is important for understanding the features of their interaction with the environment. Such beams are characterized by the presence of orbital angular momentum, which affects their behavior during propagation. In free space vortices can demonstrate the stability of the wave front structure, which allows them to preserve their unique properties over long distances [19, 20].

Focusing of vortex laser beams in the terahertz range is a complex and at the same time promising area of research. Focused beams have unique properties that can be used to create super-dense foci, compact foci with dimensions below the diffraction limit, optical needles, light tunnels, flat-top foci, focal matrices, and others [21 – 23]. There are only a few works known in which the focusing of vortex beams in the terahertz range is studied. In [24, 25], a series of terahertz emitters with a spiral Fresnel zone plate was developed for direct generation of focused terahertz vortex beams. The authors [26, 27] proposed metasurfaces that can be used to focus incident waves with arbitrary polarization states into vortex beams carrying a certain topological charge.

Cite as: A.V. Degtyarev, M.M. Dubinin, V.A. Maslov, K.I. Muntean, O.O. Svystunov, East Eur. J. Phys. 3, 93 (2025), https://doi.org/10.26565/2312-4334-2025-3-09

It is well known that terahertz optically pumped molecular lasers have the advantages of high power, room temperature operation, and long-term stability over other practical terahertz radiation sources. Most optically pumped lasers use waveguide resonators, which make it possible to obtain sufficiently high powers (up to 1 W) in a continuous mode with relatively small cavity sizes [28]. Among the modes of such resonators the TM_{01} mode with radial field polarization, which has the lowest losses in this class of modes, is of interest.

A spiral phase plate (SPP) with an azimuthally varying thickness is one of the most well-known optical elements for the formation of vortex beams [29, 30]. The SPP works by directly imposing a helical phase shift on the incident laser beam, allowing almost 100 % of the incident radiation energy to be converted into the optical beam.

The aim of this work is to obtain analytical expressions for describing nonparaxial diffraction during propagation and focusing in free space of wave beams excited by the TM_{01} mode with radial polarization of the field of the waveguide resonator of a terahertz laser, during its interaction with a spiral phase plate. In addition, using numerical modeling, this work studies the physical properties of the resulting vortex beams during their propagation in free space and tight focusing.

2. THEORETICAL RELATIONSHIPS

We describe the propagation of laser radiation in free space along the 0*z* axis using the well-known integral Rayleigh-Sommerfeld transformations **[**31 – 33**].** In a cylindrical coordinate system, we use the following expressions for the field components in different diffraction zones

$$E_r(\rho_1,\beta,z_1) = -\frac{i z_1}{\lambda r_1^2}\exp(ikr_1)\int_0^{\infty}\int_0^{2\pi}[E_r^0(\rho_0,\varphi)\cos(\varphi-\beta) - E_\varphi^0(\rho_0,\varphi)\sin(\varphi-\beta)]\times \\ \times \exp\left(ik\frac{\rho_0^2}{2r_1}\right)\exp\left[-ik\frac{\rho_1\rho_0\cos(\varphi-\beta)}{r_1}\right]\rho_0\, d\rho_0\, d\varphi, \tag{1.1}$$

$$E_\varphi(\rho_1,\beta,z_1) = -\frac{i z_1}{\lambda r_1^2}\exp(ikr_1)\int_0^{\infty}\int_0^{2\pi}[E_r^0(\rho_0,\varphi)\sin(\varphi-\beta) + E_\varphi^0(\rho_0,\varphi)\cos(\varphi-\beta)]\times \\ \times \exp\left(ik\frac{\rho_0^2}{2r_1}\right)\exp\left[-ik\frac{\rho_1\rho_0\cos(\varphi-\beta)}{r_1}\right]\rho_0\, d\rho_0\, d\varphi, \tag{1.2}$$

$$E_z(\rho_1,\beta,z_1) = \frac{-i}{\lambda r_1^2}\exp(ikr_1)\int_0^{\infty}\int_0^{2\pi}\left\{E_r^0(\rho_0,\varphi)[\rho_0 - \rho_1\cos(\varphi-\beta)] + E_\varphi^0(\rho_0,\varphi)\rho_1\sin(\varphi-\beta)\right\}\times \\ \times \exp\left(ik\frac{\rho_0^2}{2r_1}\right)\exp\left[-ik\frac{\rho_1\rho_0\cos(\varphi-\beta)}{r_1}\right]\rho_0\, d\rho_0\, d\varphi, \tag{1.3}$$

where $k = 2\pi/\lambda$ is the wave number, λ is the wavelength, (ρ_0,φ) are the polar coordinates in the area where the input field is specified, (ρ_1,β,z_1) are the cylindrical coordinates in the observation plane, $E_r^0(\rho_0,\varphi)$ and $E_\varphi^0(\rho_0,\varphi)$ are the complex amplitudes *r* and φ components of the input electric field, $r_1 = \sqrt{\rho_1^2 + z_1^2}$.

The modes of the studied dielectric resonator coincide with the modes of a hollow circular dielectric waveguide. Therefore, in the initial plane we specify radiation in the form of a symmetrical radially polarized TM_{01} mode. The normalized expressions for the cylindrical components of the electromagnetic field of this mode in the source plane $z = 0$ have the following form [34]

$$\mathrm{TM}_{01}\ \text{mode}\ \begin{cases} E_r^0(\rho_0,\varphi) = B_{01}J_1\left(U_{01}\dfrac{\rho_0}{a}\right), \\ E_\varphi^0(\rho_0,\varphi) = 0, \end{cases} \tag{2}$$

where *a* is the waveguide radius, J_1 is the Bessel function of the 1st kind of the first order, U_{01} is the first root of the equation $J_1(x) = 0$, $B_{01} = \dfrac{1}{a\sqrt{\pi}J_0(U_{01})}$ is the normalizing factor for TM_{01} mode.

Let us consider the interaction between of this mode and a spiral phase plate with its arbitrary topological charge (*n*) [35]. The SPP is positioned at the output of a waveguide with an aperture of the same diameter (Figure 1). The complex transmission function of this SPP with a radius *a* in polar coordinates has the form [36]:

$$T_n(\rho_0,\varphi)=\mathrm{circ}\left(\frac{\rho_0}{a}\right)\exp(in\varphi), \tag{3}$$

where circ(·) is the circular function.

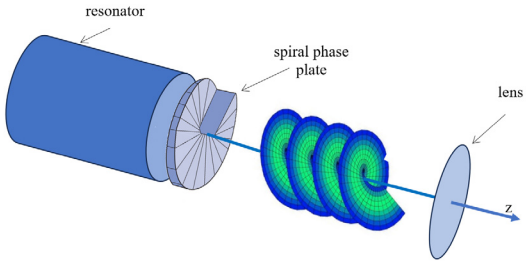

Figure 1. Topology of the model.

For simplifying calculations, integration over the angle φ in (1) can be performed using known relations for the integer $m \geq 0$ from [32]

$$\int_0^{2\pi}\cos(m\varphi+\varphi_0)\exp[-ix\cos(\varphi-\theta)d\varphi]=2\pi(-i)^m J_m(x)\cos(m\theta+\varphi_0)\ ,$$

$$\int_0^{2\pi}\sin(m\varphi+\varphi_0)\exp[-ix\cos(\varphi-\theta)]\,d\varphi=2\pi(-i)^m J_m(x)\sin(m\theta+\varphi_0)\ .$$

Then from here we can obtain the following relation

$$\int_0^{2\pi} e^{-ix\cos(\varphi-\beta)}e^{in\varphi}d\varphi=2\pi\, e^{in\beta}(-i)^n J_n(x)\ . \tag{4}$$

Using Euler's formula for trigonometric functions and taking into account (4), we can obtain expressions for the following integrals:

$$\int_0^{2\pi} e^{-ix\cos(\varphi-\beta)}e^{in\varphi}\sin m\varphi\,d\varphi=-i\pi[e^{i(n+m)\beta}(-i)^{n+m}J_{n+m}(x)-e^{i(n-m)\beta}(-i)^{n-m}J_{n-m}(x)]\ , \tag{5.1}$$

$$\int_0^{2\pi} e^{-ix\cos(\varphi-\beta)}e^{in\varphi}\cos m\varphi\,d\varphi=\pi\,[e^{i(n+m)\beta}(-i)^{n+m}J_{n+m}(x)+e^{i(n-m)\beta}(-i)^{n-m}J_{n-m}(x)]\ , \tag{5.2}$$

$$\int_0^{2\pi} e^{-ix\cos(\varphi-\beta)}e^{in\varphi}\sin(\varphi-\beta)\,d\varphi=\pi(-i)^{n+2}e^{in\beta}[J_{n+1}(x)+J_{n-1}(x)]\ , \tag{5.3}$$

$$\int_0^{2\pi} e^{-ix\cos(\varphi-\beta)}e^{in\varphi}\cos(\varphi-\beta)\,d\varphi=\pi(-i)^{n+1}e^{in\beta}[J_{n+1}(x)-J_{n-1}(x)]\ . \tag{5.4}$$

Also, using formulas (5.1 – 5.4), we obtain expressions for the field components describing the nonparaxial diffraction of vortex beams excited by the TM_{01} mode in free space. They have the following form:

$$E_r(\rho_1,\beta,z_1)=\frac{(-i)^{n+2}k\,z_1}{2r_1^2}e^{i(n\beta+kr_1)}B_{01}[I1_{1n+1}(\rho_1,z_1)-I1_{1n-1}(\rho_1,z_1)]\ , \tag{6.1}$$

$$E_\varphi(\rho_1,\beta,z_1)=\frac{(-i)^{n+3}k\,z_1}{2r_1^2}e^{i(n\beta+kr_1)}B_{01}[I1_{1n+1}(\rho_1,z_1)+I1_{1n-1}(\rho_1,z_1)]\ , \tag{6.2}$$

$$E_z(\rho_1,\beta,z_1)=\frac{(-i)^{n+1}k}{2r_1^2}e^{i(n\beta+kr_1)}B_{01}\{2\,I2_{1n}(\rho_1,z_1)+i\rho_1[I1_{1n+1}(\rho_1,z_1)-I1_{1n-1}(\rho_1,z_1)]\}\ , \tag{6.3}$$

where the following notations are introduced

$$I1_{1n}(\rho_1,z_1)=\int_0^a J_1\left(U_{01}\frac{\rho_0}{a}\right)\,J_n\left(\frac{k\rho_1\rho_0}{r_1}\right)\,\exp\left(ik\frac{\rho_0^2}{2r_1}\right)\rho_0\,d\rho_0\ ,$$

$$I2_{1n}(\rho_1, z_1) = \int_0^a J_1\left(U_{01}\frac{\rho_0}{a}\right) J_n\left(\frac{k\,\rho_1\,\rho_0}{r_1}\right)\exp\left(ik\frac{\rho_0^2}{2r_1}\right)\rho_0^2\,d\rho_0.$$

The field at the input and output of a lens with radius a_1 is described using the phase correction function [37] $U(\rho_1) = \exp\left(\frac{-i\pi\rho_1^2}{\lambda F}\right)$, where F is the focal length of a lens. By repeatedly applying the Rayleigh-Sommerfeld integral transformations (1) to the components of the electric field strength vector (6) found after phase correction, we obtain analytical expressions for the transverse and longitudinal components of the field in the focal region of the lens. These expressions for the components of the field of the vortex beam excited by the radially polarized TM_{01} mode at a distance z_2 from the lens have the form

$$E_r(\rho_2,\theta,z_2) = \frac{(-i)^{2n}k^2\,z_1z_2}{2r_2^2}\exp[i(n\theta+kr_2)]B_{01}\times$$
$$\times\int_0^{a_1}\left[I1_{1n+1}(\rho_1,z_1)J_{n+1}(x)+I1_{1n-1}(\rho_1,z_1)J_{n-1}(x)\right]\frac{\exp[ik(r_1+\frac{\rho_1^2}{2r_2})]}{r_1^2}U(\rho_1)\rho_1 d\rho_1, \quad (7.1)$$

$$E_\varphi(\rho_2,\theta,z_2) = \frac{(-i)^{2n+1}k^2\,z_1z_2}{2r_2^2}\exp[i(n\theta+kr_2)]B_{01}\times$$
$$\times\int_0^{a_1}\left[[I1_{1n+1}(\rho_1,z_1)J_{n+1}(x)-I1_{1n-1}(\rho_1,z_1)J_{n-1}(x)]\right]\frac{\exp[ik(r_1+\frac{\rho_1^2}{2r_2})]}{r_1^2}U(\rho_1)\rho_1 d\rho_1, \quad (7.2)$$

$$E_z(\rho_2,\theta,z_2) = \frac{(-i)^{2n-1}k^2\,z_1}{2r_2^2}\exp[i(n\theta+kr_2)]B_{01}\times$$
$$\times\int_0^{a_1}\left\{\rho_1 J_n(x)[I1_{1n+1}(\rho_1,z_1)-I1_{1n-1}(\rho_1,z_1)]+i\rho_2[I1_{1n+1}(\rho_1,z_1)J_{n+1}(x)+I1_{1n-1}(\rho_1,z_1)J_{n-1}(x)\right\}\times \quad (7.3)$$
$$\times\frac{\exp[ik(r_1+\frac{\rho_1^2}{2r_2})]}{r_1^2}U(\rho_1)\rho_1 d\rho_1.$$

3. NUMERICAL RESULTS AND DISCUSSIONS

Using the obtained expressions, calculations were carried out to determine the distribution of the total intensity ($I=|E_r|^2+|E_\varphi|^2+|E_z|^2$) as well as the intensity and phase ($\varphi = \mathrm{arctg}(\mathrm{Im}(E_i)/\mathrm{Re}(E_i)), i = x, y, z$) of individual field components of vortex laser beams excited by a radially polarized TM_{01} mode of a dielectric waveguide resonator of a terahertz laser, as they propagate in free space and under tight focus conditions. In the calculations the radiation wavelength was $\lambda = 0.4326$ mm, which corresponds to the generation line of a formic acid (HCOOH) terahertz laser with optical pumping [38]. The SPP was placed at the output of the waveguide resonator and formed the investigated vortex laser beams. The waveguide and SPP had identical diameters of $2a = 35$ mm, and the lens diameter was $2a_1 = 50$ mm. The focal length of the lens was $F = 36.36$ mm [39, 40] which provided the conditions for tight focusing (the numerical aperture of the lens was NA = 0.68, where NA = a_1 / F).

Figure 2 shows the longitudinal intensity distributions of the field (a1 – a3), as well as the transverse intensity distributions in the regions of maximum field intensity (b1 – b3) for laser beams without SPP ($n = 0$) and vortex beams ($n = 1, 2$) in free space. The longitudinal field intensity distributions are presented in the Fresnel diffraction zone for $z_1 = 100 – 1000$ mm.

From Figure 2 (a1, b1) it can be seen that for SPP with a topological charge of $n = 0$ in the absence of a phase plate the investigated beam has a ring-like shape in the cross-section. The maximum intensity I_{max} of the laser beam at $n = 0$ is observed at a distance of $z_1 = 175$ mm from SPP and it is equal to 0.0023 absolute units, which corresponds to the intensity at the output mirror of the waveguide resonator. The I_{max} values in the regions of maximum intensity remain almost unchanged when using SPP. Additionally, at the distances where the maximum intensity regions are observed, the effective beam diameter d_s was calculated for different topological charges using the formula:

$$d_s = 2\sqrt{\frac{2\int_0^{2\pi}\int_0^{\infty}\rho_1^2 I(\rho_1,\beta,z_1)\rho_1 d\rho_1 d\beta}{\int_0^{2\pi}\int_0^{\infty} I(\rho_1,\beta,z_1)\rho_1 d\rho_1 d\beta}}. \quad (8)$$

The value of d_s in the region of maximum intensity (z_1 = 175 mm) for n = 0 is equal to 21 mm.

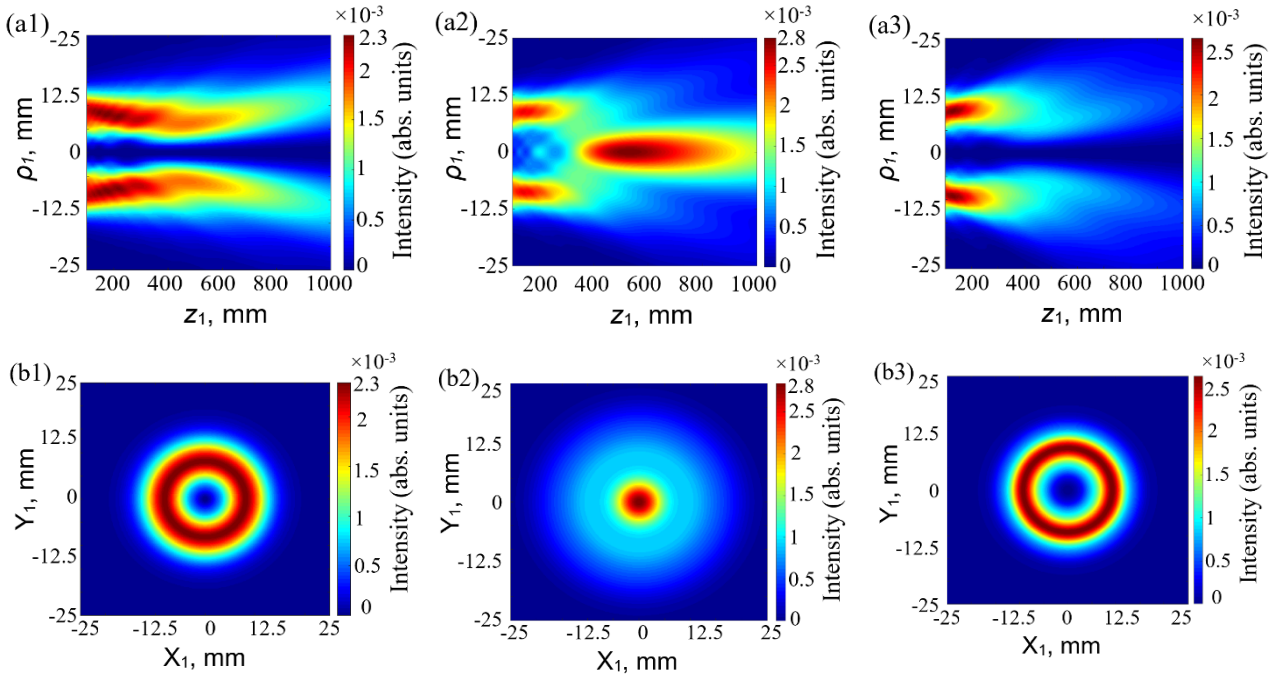

Figure 2. Longitudinal intensity distributions of the field (a1 – a3), as well as transverse intensity distributions in the regions of maximum field intensity (b1 – b3) for different values of the topological charge in free space. The first, second and third columns correspond to n = 0, n = 1 and n = 2, respectively.

The use of SPP with a topological charge of n = 1 at the waveguide output leads to a change in the beam profile from a ring-shaped structure to a profile with a field maximum on the axis (Figure 2 (b2)). This behavior of the beam profile change is due to the fact that, as can be seen from the integral expressions for the field components (6.1 – 6.3), these components have a minimum on the axis in the absence of SPP at the waveguide output. When SPP with n = 1 is installing, these field components reach their maximum value on the axis due to the influence of the second term in the expressions for these components. In this case the region of maximum intensity shifts to a distance of z_1 = 527 mm from SPP (Figure 2 (a2) and the effective beam diameter increases to d_s = 27.5 mm.

A subsequent change in the value of the topological charge (n = 2) leads to a zero value of these field components on the axis. As the topological charge increases from n = 1 to n = 2, the beam profile restores its initial ring-shaped structure (Figure 2 (a3, b3)). The region of maximum intensity is located at a distance of z_1 = 130.5 mm (Figure 2 (a3)), and the effective beam diameter d_s in this region, as in the absence of SPP, is equal to 21 mm.

Additionally, the dependencies of the relative contribution η of the field components to the power of the laser beam in the Fresnel diffraction zone were calculated for topological charges n = 1, 2 according to the formula:

$$\eta(z_1) = \frac{\int_0^{2\pi}\int_0^{\infty}\left|E_{r,\phi,z}(\rho_1,\beta,z_1)\right|^2 \rho_1 d\rho_1 d\beta}{\int_0^{2\pi}\int_0^{\infty}\left[\left|E_r(\rho_1,\beta,z_1)\right|^2 + \left|E_\phi(\rho_1,\beta,z_1)\right|^2 + \left|E_z(\rho_1,\beta,z_1)\right|^2\right]\rho_1 d\rho_1 d\beta}. \quad (9)$$

In the absence of SPP the total field intensity is determined by the radial E_r component. The contribution of the E_z component to the total beam power is negligible; therefore, the graph of the field components contribution to the laser beam power is not presented.

The results of calculations of the dependence of the relative contribution η of the field components to the power of the laser beam during its propagation in free space for topological charges of SPP n = 1, 2 are shown in Figure 3. For n = 1 the contribution of the radial E_r component decreases with increasing distance from SPP, while the contribution of the azimuthal component E_φ gradually increases and begins to dominate at large distances (Figure 3a). The contribution of the longitudinal component E_z remains practically constant and has a negligible effect on the beam power over the entire studied range. For n = 2 an increase in the contribution of the azimuthal component to the beam power is observed, indicating a growing role of this component with increasing topological charge (Figure 3b).

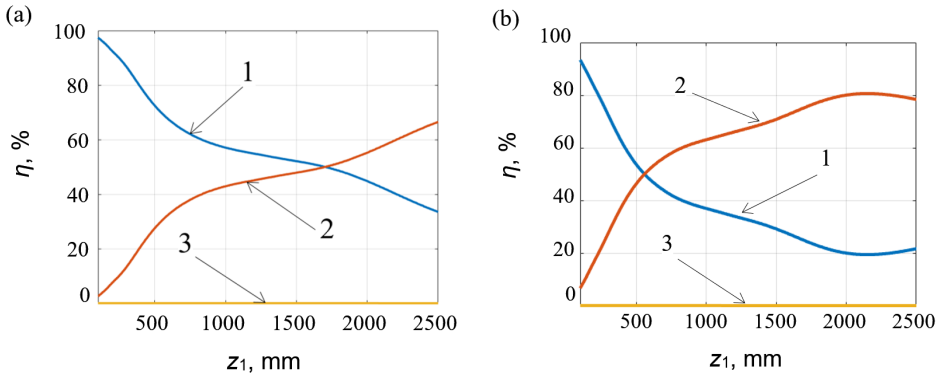

Figure 3. Dependencies of the relative contribution η of the field components (1 – E_r, 2 – E_φ, 3 – E_z) to the power of the vortex laser beam on the function of the distance z_1 from SPP for topological charges n = 1 (a), n = 2 (b).

The spatial-energy characteristics of vortex laser beams in the focal region of the lens were also studied under the condition of tight focusing. A short focal length lens (F = 36.36 mm) was installed in the region of maximum field intensity for different topological beam charges to fulfill this condition. The longitudinal field intensity distributions of laser beams for various topological charge values (n = 0, 1, 2) are shown in Figure 4. The figures indicate that the maximum intensity value for these topological charges is observed at n = 1 and reaches 2.2 absolute units (Figure 4b).

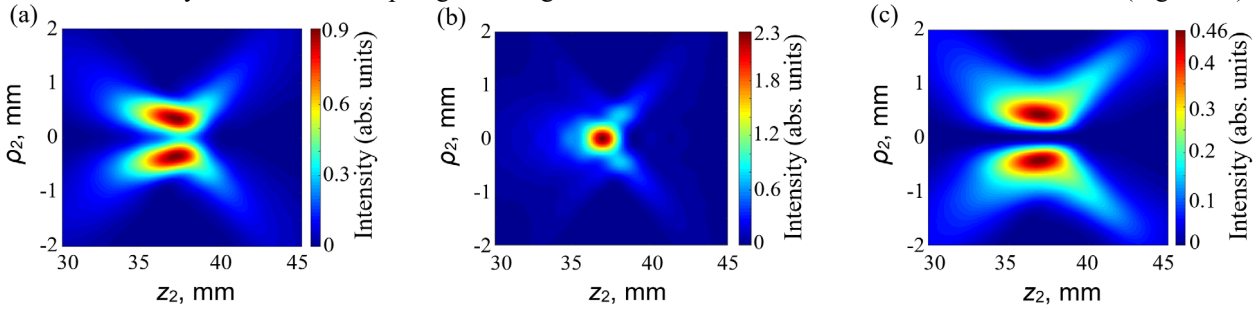

Figure 4. Longitudinal field intensity distributions of the laser beam without SPP (n = 0) and vortex beams (n = 1, 2) in the focal region of the lens.

The dependencies of the relative contribution η of the electric field components for focused laser beams to their total power were calculated for different topological charges. The results are shown in Figure 5.

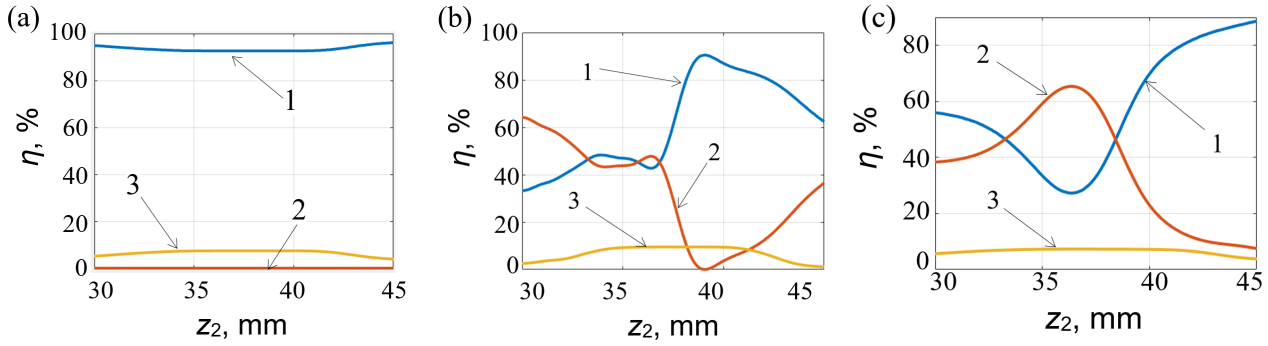

Figure 5. Dependencies of the relative contribution η of the field components (1 – E_r, 2 – E_φ, 3 – E_z) to the power of the laser beam without SPP (n = 0) and vortex beams (n = 1, 2) on the function of the distance z_2 from the lens.

In the case of zero topological charge the radial component is dominant, which maintains a stable high level of relative contribution $\eta \approx 90$ % throughout the entire range of the focal region (Figure 5a). The contribution of the azimuthal component in this case is zero, and the longitudinal component has a small increase in the central part of the focal region, not exceeding 10 % of the beam total power. The introduction of a topological charge into the beam (n = 1) leads to a

significant redistribution of energy in the beam between the radial and azimuthal components of the electric field in the focal region (Figure 5b). The contribution of the azimuthal component is dominant at distances $z_2 \approx 30 - 35$ mm to the geometric focus, while the radial component has a smaller contribution to the total beam power in this region. However, the contribution of the azimuthal component significantly changes at a distance $z_2 \approx 36 - 40$ mm, while the contribution of the radial component begins to grow and reaches a maximum after the geometric focus of the lens. The contribution of the longitudinal component to the beam power, as in the case of $n = 0$, remains insignificant but it shows growth in the region of the geometric focus. The redistribution of the contribution to the total beam power for the radial and azimuthal components is observed even more for the topological beam charge $n = 2$. The contribution of the longitudinal component also shows an increase in the geometric focus region of the lens (Figure 5c).

Figure 6 shows the spatial transverse distributions of the total intensity, as well as the intensity and phase of individual components of the electric field for a tightly focused laser beam in the absence of SPP. In this case the total intensity distribution has a ring-shaped structure. However, there is a small field intensity on the axis (Figure 6(a1)), which is caused by the influence of the longitudinal component (Figure 6 (b2)). In this case the azimuthal component is zero. The phase front of both components is spherical (Figure 6 (c1, c2)), which is explained by the absence of orbital angular momentum in the radiation. As a result of focusing the effective beam diameter d_f defined similarly (8) in the region of maximum intensity ($z_2 = 37$ mm) decreases to $d_f = 2.4$ mm compared to the beam diameter d_s during propagation in free space ($z_1 = 175$).

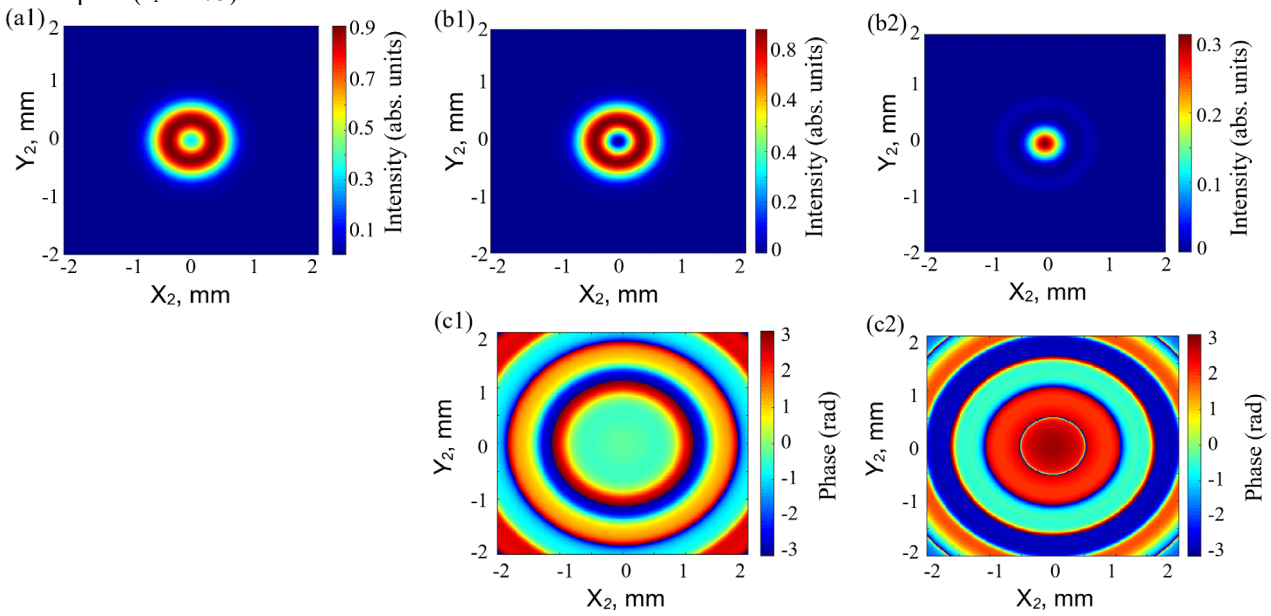

Figure 6. Transverse distributions of the total field intensity (a1), as well as the intensity (b1, b2) and phase (c1, c2) of the field for the E_r (b1, c1) and E_z (b2, c2) components of a tightly focused laser beam in the absence of SPP.

Analysis of the vortex laser beam for $n = 1$ shows that the total intensity distribution has a maximum on the axis (Figure 7(a1)).

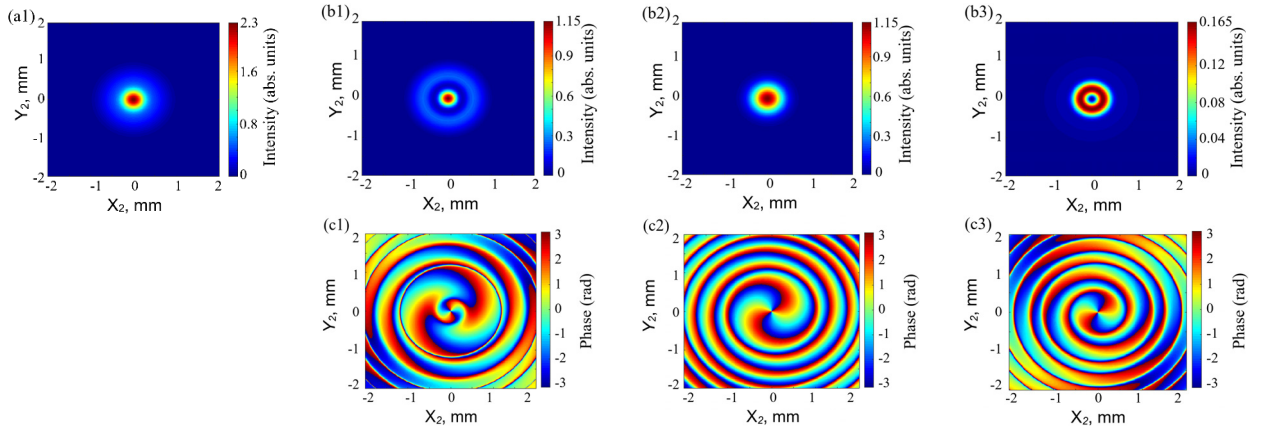

Figure 7. Transverse distributions of the total field intensity (a1), as well as the intensity (b1 – b3) and phase (c1 – c3) of the field for the E_r (b1, c1), E_ϕ (b2, c2) and E_z (b3, c3) components of a tightly focused vortex laser beam with a topological charge of $n = 1$.

The effective beam diameter d_f at $z_2 = 37$ mm compared to the beam diameter d_s during propagation in free space decreases to $d_f = 1.0$ mm. Radial and azimuthal components make equal contributions to the field intensity distribution

in the region of geometric focus (Figure 7 (b1, b2)). Meanwhile, the longitudinal component exhibits a ring-shaped field distribution and has almost no effect on the total intensity (Figure 7 (b3)). The phase distribution of all three field components represents a vortex with two branches (Figure 7 (c1 – c3)).

For the beam with a topological charge of $n = 2$ the total field intensity distribution has a pronounced ring-shaped structure (Figure 8 (a1)). The transverse intensity distribution for all three field components also has a ring-shaped profile in the focal region (Figure 8 (b2 – b3)). The effective beam diameter d_f at $z_2 = 37$ mm decreases to $d_f = 3.7$ mm compared to the beam diameter d_s during propagation in free space. The phase distribution of all three components shows the presence of a vortex with four branches (Figure 8 (c1 – c3)).

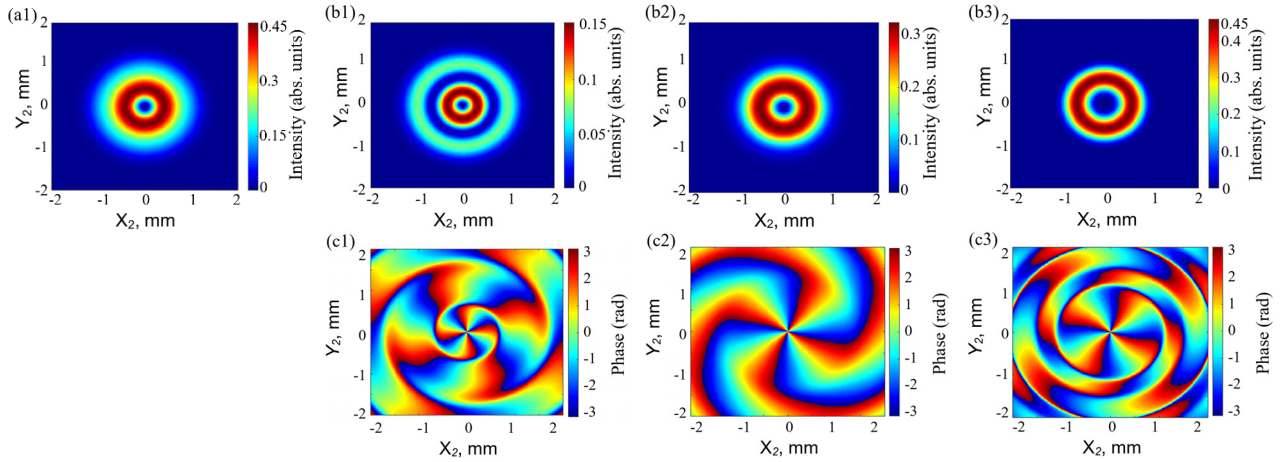

Figure 8. Transverse distributions of the total field intensity (a1), as well as the intensity (b1 – b3) and phase (c1 – c3) of the field for the E_r (b1, c1), E_ϕ (b2, c2) and E_z (b3, c3) components of a tightly focused vortex laser beam with a topological charge of $n = 2$

3. CONCLUSIONS

Analytical expressions have been obtained that describe nonparaxial diffraction in free space of the TM_{01} mode with radial polarization of the field of the dielectric resonator of a waveguide terahertz laser during its interaction with a spiral phase plate with different topological charges (n). Physical features of the obtained vortex beams during their propagation in free space and tight focusing are studied by numerical modeling.

It is shown that the use of SPP at the waveguide output with a topological charge $n = 1$ leads to a change in the beam profile during its propagation in free space from a ring-shaped beam to a beam having a field maximum on the axis. A subsequent change in the value of the topological charge ($n = 2$) leads to a zero value of these field components on the axis. In the absence of a spiral phase plate the total intensity of the beam field is determined by the radial and longitudinal components, whereas in its presence it is determined by all three components of the field.

The distribution of the total field intensity in the absence of a spiral phase plate has a ring structure with tight focusing. At the same time a slight field intensity is observed on the axis due to the contribution of the longitudinal component. The total distribution of field intensity has a maximum on the axis and the effective beam diameter d_f reaches a minimum value of 1 mm when using SPP with a topological charge $n = 1$. In this case the phase distribution of the field components is characterized by the presence of two vortices. For the beam with a topological charge of $n = 2$ the distribution of the total intensity has a clearly defined ring structure and the phase distribution of the field components demonstrates the presence of four vortices.

Declarations

Conflict of interest. None declared.
Ethical approval. Not required.

ORCID

Andrey V. Degtyarev, https://orcid.org/0000-0003-0844-4282; **Mykola M. Dubinin,** https://orcid.org/0000-0002-7723-9592
Vyacheslav O. Maslov, https://orcid.org/0000-0001-7743-7006; **Konstantin I. Muntean,** https://orcid.org/0000-0001-6479-3511
Oleh O. Svystunov, https://orcid.org/0000-0002-4967-5944

REFERENCES

[1] G.S. Park, M. Tani, J.S. Rieh, and S.Y. Park, *Advances in Terahertz Source Technologies*, (CRC Press, 2024).
[2] A. Saha, A. Biswas, K. Ghosh, and N. Mukhopadhyay, *Optical to Terahertz Engineering*, (Springer, 2023).
[3] B. Gu, Y. Hu, X. Zhang, M. Li, Z. Zhu, G. Rui, and Y. Cui, "Angular momentum separation in focused fractional vector beams for optical manipulation", Optics Express, **29**(10), 14705 (2021). https://doi.org/10.1364/OE.423357
[4] B. Gao, J. Wen, G. Zhu, L. Ye, and L.G. Wang, "Precise measurement of trapping and manipulation properties of focused fractional vortex beams", Nanoscale, **14**(8), 3123 (2022). https://doi.org/10.1039/D1NR06163A
[5] B. Pant, B.K. Mishra, S. Singh, and B.K. Singh, "Mode transformation and dark spot formation of cylindrical vector beams by thin dielectric film", Optics & Laser Technology, **180**, 111539 (2025). https://doi.org/10.1016/j.optlastec.2024.111539

[6] J. Ma, Z. Xie, and X. Yuan, "Tailoring arrays of optical stokes skyrmions in tightly focused beams", Laser & Photonics Reviews, **19**(3), 2401113 (2025). https://doi.org/10.1002/lpor.202401113
[7] M. Liu, Y. Lei, L. Yu, X. Fang, Y. Ma, L. Liu, and P. Gao, "Super-resolution optical microscopy using cylindrical vector beams", Nanophotonics, **11**(15), 3395 (2022). https://doi.org/10.1515/nanoph-2022-0241
[8] X. Yuan, H. Guo, S. Zhuang, and J. Hu, "Generation and high-resolution focusing of higher-order vector beam via metasurface", IEEE Photonics Journal, **16**, 2201206 (2024). https://doi.org/10.1109/JPHOT.2024.3406534
[9] S. Boichenko, "Fast-speed algorithm to compute tight focusing of laser beams: Effectiveness of circularly polarized vortex beam series as a mathematical basis", Physical Review A, **109(**4), 043501 (2024). https://doi.org/10.1103/PhysRevA.109.043501
[10] V.V. Kotlyar, S.S. Stafeev, V.D. Zaitsev, A.M. Telegin, and E.S. Kozlova, "Spin–orbital transformation in a tight focus of an optical vortex with circular polarization", Applied Sciences, **13(**14), 8361 (2023). https://doi.org/10.3390/app13148361
[11] Y. Miao, L. Wang, Q. Zhang, X. Sun, X. Gao, J. Wan, and S. Zhuang, "Tight-focusing properties of propagable fractional-order vector vortex beams", Journal of the Optical Society of America B, **40(**5), 1113 (2023). https://doi.org/10.1364/JOSAB.485509
[12] D. Maluenda, M. Aviñoá, K. Ahmadi, R. Martínez-Herrero, and A. Carnicer, "Experimental estimation of the longitudinal component of a highly focused electromagnetic field", Scientific Reports, **11(**1), 17992 (2021). https://doi.org/10.1038/s41598-021-97164-z
[13] Z. Qing, W. Yan, X. Long, Z. Yuan, Z.C. Ren, X.L. Wang, and H.T. Wang, "Longitudinal manipulation of local nonseparability in vector beams", Optics Letters, **49(**10), 2557 (2024). https://doi.org/10.1364/OL.524647
[14] D.A. Ikonnikov, S.A. Vyunisheva, D.V. Prokopova, N.N. Losevsky, S.A. Samagin, S.P. Kotova, and A.M. Vyunishev, "Configurable vortex laser beams for optical manipulations of microparticle ensembles", Laser Physics Letters, **20(**8), 086002 (2023). https://doi.org/10.1088/1612-202X/ace0af
[15] J. Zeng, Y. Dong, Y. Wang, J. Zhang, and J. Wang, "Optical imaging using orbital angular momentum: interferometry, holography and microscopy", Journal of Lightwave Technology, **41(**7), 2025 (2022). https://doi.org/10.1109/JLT.2022.3225214
[16] M. Cheng, W. Jiang, L. Guo, J. Li, and A. Forbes, "Metrology with a twist: probing and sensing with vortex light", Light: Science & Applications, **14(**1), 4 (2025). https://doi.org/10.1038/s41377-024-01665-1
[17] F. Pang, L. Xiang, H. Liu, L. Zhang, J. Wen, X. Zeng, and T. Wang, "Review on fiber-optic vortices and their sensing applications", Journal of Lightwave Technology, **39(**12), 3740 (2021). https://opg.optica.org/jlt/abstract.cfm?URI=jlt-39-12-3740
[18] S.K. Noor, M.N.M. Yasin, A.M. Ismail, M.N. Osman, P.J. Soh, N.Ramli, and A.H. Rambe, "A review of orbital angular momentum vortex waves for the next generation wireless communications", Ieee Access, **10**, 89465 (2022). https://doi.org/10.1109/ACCESS.2022.3197653
[19] D. Bongiovanni, D. Li, M. Goutsoulas, H. Wu, Y. Hu, D. Song, and Z. Chen, "Free-space realization of tunable pin-like optical vortex beams", Photonics Research, **9(**7), 1204 (2021). https://doi.org/10.1364/PRJ.420872
[20] G. Wang, X. Weng, X. Kang, Z. Li, K. Chen, X. Gao, and S. Zhuang, "Free-space creation of a perfect vortex beam with fractional topological charge", Optics Express, **31(**4), 5757 (2023). https://doi.org/10.1364/OE.483304
[21] Z. Shen, and S. Huang, "Generation of subdiffraction optical needles by simultaneously generating and focusing azimuthally polarized vortex beams through Pancharatnam–Berry metalenses", Nanomaterials, **12(**22), 4074 (2022). https://doi.org/10.3390/nano12224074
[22] J. Chen, and Q. Xu, "Superlong uniform light tunnel created by focusing radially polarized vortex beam", Journal of Applied Physics, **124**, 4 (2018). https://doi.org/10.1063/1.5033926
[23] P.B. Singh, and B. Kumar, "Formation of subwavelength tunable flat-top focus with double foci characteristic by tightly focused cylindrical vector beams", Optics Communications, **572**, 130972 (2024). https://doi.org/10.1016/j.optcom.2024.130972
[24] X. Zhang, Y. Xu, B. Hong, F. Zhang, A. Wang, and W. Zhao, "Generation of a focused THz vortex beam from a spintronic THz emitter with a helical Fresnel zone plate", Nanomaterials. **13(**14), 2037 (2023). https://doi.org/10.3390/nano1314203
[25] X. Feng, X. Chen, Y. Lu, Q. Wang, L. Niu, Q. Xu, and W. Zhang, "Direct emission of focused terahertz vortex beams using Indium-Tin-Oxide-based Fresnel zone plates", Advanced Optical Materials, **11**(1), 2201628 (2023). https://doi.org/10.1002/adom.202201628
[26] M. Zhong, and J.S. Li, "Terahertz vortex beam and focusing manipulation utilizing a notched concave metasurface", Optics Communications, **511**, 127997 (2022). https://doi.org/10.1016/j.optcom.2022.127997
[27] H. Li, C. Zheng, H. Xu, J. Li, C. Song, F. Yang, and J. Yao, "All-graphene geometric terahertz metasurfaces for generating multi-dimensional focused vortex beams", Opt. Laser Technol, **159,** 108986 (2023). https://doi.org/10.1016/j.optlastec.2022.108986
[28] J. Farhoomand, and H.M. Pickett, "Stable 1.25 watts CW far infrared laser radiation at the 119 μm methanol line", Int. J. Infrared Millim. Waves, **8**, 441 (1987). https://doi.org/10.1007/BF01013257
[29] M.W. Beijersbergen, R.P.C. Coerwinkel, M. Kristensen, and J.P. Woerdman, "Helical-wavefront laser beams produced with a spiral phase plate", Opt. Commun., **112**(5-6), 321 (1994). https://doi.org/10.1016/0030-4018(94)90638-6
[30] A.V. Ustinov, S.N. Khonina, P.A. Khorin, and A.P. Porfirev, "Control of the intensity distribution along the light spiral generated by a generalized spiral phase plate", Journal of the Optical Society of America B, **38(**2), 420 (2021). https://doi.org/10.1364/JOSAB.408884
[31] V.V. Kotlyar, and A.A. Kovalev, "Nonparaxial propagation of a Gaussian optical vortex with initial radial polarization", J. Opt. Soc. Am. A, **27**(3), 372 (2010). https://doi.org/10.1364/JOSAA.27.000372
[32] B. Gu, and Y. Cui, "Nonparaxial and paraxial focusing of azimuthal-variant vector beams", Opt. Express, **20**(16), 17684 (2012). https://doi.org/10.1364/OE.20.017684
[33] Y. Zhang, L. Wang, and C. Zheng, "Vector propagation of radially polarized Gaussian beams diffracted by an axicon", J. Opt. Soc. Am. A, **22**(11), 2542 (2005). https://doi.org/10.1364/JOSAA.22.002542
[34] E.A.J. Marcatili, and R.A. Schmeltzer, "Hollow metallic and dielectric waveguides for long distance optical transmission and lasers", Bell Syst. Tech. J., **43(**4), 1783 (1964). https://doi.org/10.1002/j.1538-7305.1964.tb04108.x
[35] J.F. Nye, and M.V. Berry, "Dislocations in wave trains", Proceedings of the Royal Society of London. A. Mathematical and Physical Sciences, **336**(1605), 165 (1974). https://doi.org/10.1098/rspa.1974.0012
[36] H. Wang, Q. Song, Y. Cai, Q. Lin, X. Lu, H. Shangguan, Y. Ai, and S. Xu, "Recent advances in generation of terahertz vortex beams and their applications", Chin. Phys. B, **29**(9), 097404 (2020). https://doi.org/10.1088/1674-1056/aba2df

[37] J.W. Goodman, *Introduction to Fourier optics*, (Roberts and Company Publishers, 2005).
[38] O.V. Gurin, A.V. Degtyarev, N.N. Dubinin, M.N. Legenkiy, V.A. Maslov, K.I. Muntean, V.N. Ryabykh and V.S. Senyuta, "Formation of beams with nonuniform polarisation of radiation in a cw waveguide terahertz laser", Quantum Electron., **51**(4), 338 (2021). https://doi.org/10.1070/QEL17511
[39] A.V. Degtyarev, M.M. Dubinin, O.V. Gurin, V.A. Maslov, K.I. Muntean, V.N. Ryabykh, V.S. Senyuta, "Control of tightly focused laser beams in the THz range", Microwave and Optical Technology Letters, **63**(11), 2888 (2021). https://doi.org/10.1002/mop.32946
[40] A.V. Degtyarev, M.M. Dubinin, O.V. Gurin, V.A. Maslov, K.I. Muntean, V.M. Ryabykh, V.S. Senyuta, and O.O. Svystunov, "Control over higher-order transverse modes in a waveguide-based quasi-optical resonator", Radio Physics and Radio Astronomy, **27**(2**)**, 129 (2022). https://doi.org/10.15407/rpra27.02.129

ПРОСТОРОВА ДИНАМІКА РАДІАЛЬНО ПОЛЯРИЗОВАНОГО ТЕРАГЕРЦЕВОГО ЛАЗЕРНОГО ПУЧКА З ФАЗОВОЮ СИНГУЛЯРНІСТЮ

Андрій В. Дегтярьов, Микола М. Дубінін, Вячеслав О. Маслов, Костянтин І. Мунтян, Олег О. Свистунов
Харківський національний університет імені В.Н. Каразіна, майдан Свободи, 4, Харків, Україна, 61022

Отримано аналітичні вирази, що описують непараксіальну дифракцію у вільному просторі TM_{01} моди з радіальною поляризацією поля діелектричного хвилевідного резонатора терагерцового лазера при її взаємодії зі спіральною фазовою пластинкою з різним топологічним зарядом (n). Шляхом чисельного моделювання вивчено фізичні особливості отриманих вихрових пучків при їх поширенні та гострому фокусуванні. Для моделювання поширення пучків та фокусування отриманих пучків використані інтегральні дифракційні перетворення Релея–Зоммерфельда. У вільному просторі використання спіральної фазової пластинки на виході хвилеводу при топологічному заряді $n = 1$ призводить до зміни поперечного профілю пучка з кільцеподібного на пучок, який має максимум поля на осі, а далі ($n = 2$) знов на кільцеподібний. При фокусуванні розподіл сумарної інтенсивності поля за відсутності спіральної фазової пластинки має кільцеву структуру. Водночас на осі є незначна інтенсивність, що зумовлена вкладом повздовжньої компоненти поля. При використанні фазової пластинки поперечний профіль пучка змінюється так само як і при його поширенні. При цьому фазовий фронт змінюється із сферичного на спіральний з наявністю двох ($n = 1$) та чотирьох ($n = 2$) гілкових вихорів.

Ключові слова: *терагерцовий лазер; діелектричний хвилевідний резонатор; спіральна фазова пластинка; вихрові пучки; радіальна поляризація; поширення випромінювання; гостре фокусування*